Polyhedron 40 (2012) 1–10

Contents lists available at SciVerse ScienceDirect

Polyhedron

journal homepage: www.elsevier.com/locate/poly

Structural differences in eight- and ten-membered heterocyclic tin compounds displaying transannular interactions O···Sn: An experimental and theoretical study

Diego Martínez-Otero [a], Benito Flores-Chávez [b], José G. Alvarado-Rodríguez [a,*], Noemí Andrade-López [a], Julián Cruz-Borbolla [a], Thangarasu Pandiyan [b], Vojtech Jancik [c], Enrique González-Jiménez [a], Christiaan Jardinez [a]

[a] Centro de Investigaciones Químicas, Universidad Autónoma del Estado de Hidalgo, km. 4.5 Carretera Pachuca-Tulancingo, Col. Carboneras, C.P. 42184 Mineral de la Reforma, Hidalgo, Mexico
[b] Facultad de Química, Universidad Nacional Autónoma de México, Circuito Exterior, Ciudad Universitaria, C.P. 04510 D. F., México, Mexico
[c] Centro Conjunto de Investigación en Química Sustentable UAEM-UNAM, km 14.5 Carr. Toluca-Atlacomulco, Unidad San Cayetano, C.P. 50200 Toluca, Edo. de México, Mexico

ARTICLE INFO

Article history:
Received 18 January 2012
Accepted 11 April 2012
Available online 24 April 2012

Keywords:
Organotin compounds
Dithioligands
Hypercoordinated compounds
Non-bonded interactions
DFT studies

ABSTRACT

Two series of heterocyclic tin compounds of general formula $[(S\{C_6H_3(CH_2)_nS\}_2O)SnR^1R^2]$ with different central ring sizes were prepared. The ten-membered series includes the compounds with $n = 1$ and $R^1 = R^2 = Ph$ (**5**); $R^1 = Cl$, $R^2 = Ph$ (**6**); $R^1 = Cl$, $R^2 = n$-Bu (**7**); $R^1 = R^2 = Cl$ (**8**); the eight-membered series includes the compounds with $n = 0$ and $R^1 = R^2 = Ph$ (**10**); $R^1 = Cl$, $R^2 = n$-Bu (**11**) and $R^1 = R^2 = Cl$ (**12**). The compounds **5**, **7**, **8**, **10**, and **11** were investigated by single-crystal X-ray diffraction. The chloro compounds **7**, **8**, and **11** displayed a bipyramidal geometry at the tin atom with different degrees of distortion ranging from 57% to 62%. The diphenyl compounds **5** and **10** displayed a tetrahedral geometry at Sn. The conformation of the central ring in the ten-membered series is similar and is described as boat; the other series displayed two different conformations described as boat–chair and boat–boat. The possible conformers in the gas state of compounds **5**, **7**, **8**, **10**, **11**, and **12** were investigated by MMFF, LSDA, BLYP, B3LYP, and M06 functionals using the DGDZVP and TZVP basis sets. The structural data of the total optimization agreed with the experimental results. The topological analysis indicated that bond critical points are present along the O···Sn direction in the compounds **7**, **8**, **11**, and **12**.

1. Introduction

The hypercoordination through intramolecular as well as intermolecular non-covalent donor–acceptor interactions is well documented in compounds containing group 14 elements [1,2], where the donor atom is usually a Lewis base as nitrogen [3], oxygen [4] or sulfur [5]. In particular, for organotin compounds, this donor-Sn non-covalent bonding has been suggested to be important for their biological activity [6].

With respect to the hypercoordination, we are interested in the synthesis and design of ligands capable of increasing the coordination number of heavy elements of the groups 14 and 15. We have studied the coordination chemistry of dithioligands such as $\boldsymbol{D}(C_6H_4SH)_2$ [$\boldsymbol{D}$ = O, S] and the more rigid $S(C_6H_3SH)_2O$ in order to synthesize compounds of the types **I** and **II**, respectively (Scheme 1). For a given ligand, its coordination pattern can be influenced by the adequate choice of the exocyclic ligands R attached to ***A***. For the compounds of types **I** and **III**, the ***D***···***A*** interaction has recurrently been observed with several degrees of magnitude, distorting the local geometry at the central acceptor ***A*** atom; some examples are with ***A*** = Ge [7], Sn [8,9], Pb [10], As [11], and Sb [12]. In addition, it has been observed that the more electronegative are the pendant ligands R, the stronger is the interaction, leading to tridentate coordination patterns of the trichalcogenate ligand. On the other hand, in the case of the compounds of type **II** with a more rigid dithioligand, two different coordination modes have been observed in the solid state for compounds with ***A*** = Ge [13] and Pb [10]; when the acceptor atom has two organic exocyclic ligands, a bidentate coordination mode is observed and ***A*** displays a distorted tetrahedral local geometry. In the case of the germanium compounds with halogen pendant ligands where its Lewis acidity has been enhanced, the same dithioligand displays a tridentate coordination, and the acceptor Ge atom exhibits a trigonal bipyramidal coordination geometry with significantly strong O···Ge intramolecular interactions.

Following with the study of hypercoordination in the elements of the group 14, we report herein the synthesis, characterization,

* Corresponding author. Tel.: +52 771 7172000.
E-mail addresses: jgar@uaeh.edu.mx, josegalvarado@yahoo.com (J.G. Alvarado-Rodríguez).

0277-5387/$ - see front matter © 2012 Elsevier Ltd. All rights reserved.
http://dx.doi.org/10.1016/j.poly.2012.04.004

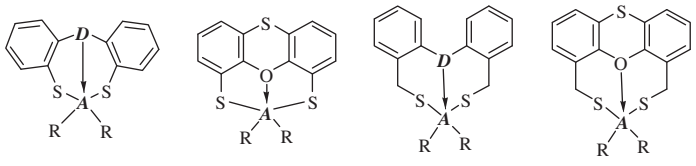

I II III IV

Scheme 1. Eight- and ten-membered heterocyclic compounds displaying transannular donor-acceptor interactions (R = alkyl, aryl, halogen, lone pair, etc.).

and theoretical studies of heterocyclic tin compounds of the types **II** (***8*-*R***** series) and **IV** (***10*-*R***** series) containing a transannular O···Sn interaction, where the flexibility of the ligands is crucial for the achievement of hypercoordination at the tin atom. The molecular and crystal structures of five compounds containing ten-membered (***10*-*R***) or eight-membered (***8*-*R***) central rings were obtained by X-ray diffraction studies. The detailed description of the synthesis, spectroscopic characterization, crystallographic data, and theoretical results is presented and discussed.

2. Experimental

2.1. Materials and physical methods

All the starting reagents such as the tin chlorides, phenoxathiin, *n*-BuLi (1.6 M, in hexanes), TMEDA, thiourea 1,4-diazabicyclo [2.2.2] octane (DABCO), $Na[BH_4]$, and $Li[AlH_4]$ were purchased from Aldrich and used as supplied. The dithioligand **9** was prepared according to the reported method [13]. All manipulations of the tin compounds, *n*-BuLi, $Li[AlH_4]$, and $Na[BH_4]$ were performed under a dry, oxygen-free dinitrogen atmosphere using standard Schlenk techniques unless noted otherwise. Solvents were dried by standard methods and distilled prior to use. Melting points were determined with a Mel-Temp II instrument and are uncorrected. The elemental analyses were recorded with a Perkin–Elmer Series II CHNS/O Analyzer. The IR spectra were recorded in the 4000–400 cm^{-1} range with a Perkin–Elmer System 2000 FT-IR spectrometer, as KBr pellets or CsI films. The ^1H, $^{13}C\{^1H\}$ and $^{119}Sn\{^1H\}$ NMR spectra were recorded on a Jeol Eclipse 400 and Varian VNMRS 400 spectrometers operating at 399.78, 100.53, and 149.03 MHz, respectively. The chemical shifts are reported in ppm with respect to the references and stated relative to external tetramethylsilane (TMS) for ^1H and ^{13}C NMR, and $SnMe_4$ for ^{119}Sn NMR spectroscopy. All the spectra were acquired at room temperature (25 °C) unless otherwise specified.

2.2. Synthesis of the dithioligand $S(C_6H_3CH_2SH)_2O$ (*4*)

The dithioligand **4** was prepared by a linear synthesis from phenoxathiin. The dialdehyde (**1**), diol (**2**), and dibromo (**3**) intermediate compounds were isolated and characterized (Scheme 2). For the chemical shifts assignments in the NMR spectroscopy of all compounds, we have used the general numbering scheme showed in the compound **4**.

2.2.1. Synthesis of $S(C_6H_3CHO)_2O$ (*1*)

A solution of *n*-BuLi 2.5 M (26 mL, 65 mmol) was slowly added to a cold solution (0 °C) of phenoxatiin (5.0 g, 25 mmol) and anhydrous TMEDA (19.4 mL, 250 mmol) in anhydrous THF (30 mL). The cold mixture was stirred for 24 h. Then, DMF (19.4 mL, 250 mmol) was then slowly added for 3 h and then refluxed for 3 h more. The cold mixture was acidified with HCl to pH 2 and extracted with dichloromethane (3 × 50 mL). The organic layers were dried with Na_2SO_4 and evaporated under reduced pressure; the yellow solid obtained was recrystallized with chloroform to yield yellow crystals. Yield: 36% (2.3 g, 9 mmol). M.p.: 237 °C. *Anal.* Calc. for $C_{14}H_8O_3S$: C, 65.61; H, 3.15. Found: C, 65.50; H, 3.14%. IR (CsI): ν = 3346, 3049, 3001, 2856, 2811, 2737, 1683, 1600, 1576, 1453, 1427, 1382, 1376, 1240, 1220, 1179, 779, 741, 716 cm^{-1}. NMR: ^1H ($CDCl_3$) δ = 10.56 s [1H, H-1], 7.68 dd [1H, H-3, $^3J_{H3-H4}$ = 7.7, $^4J_{H3-H5}$ = 1.7 Hz], 7.33 dd [1H, H-5, $^3J_{H4-H5}$ = 7.7, $^4J_{H3-H5}$ = 1.7 Hz], 7.17 td [1H, H-4, $^3J_{H3-H4}$ = 7.7, $^3J_{H4-H5}$ = 7.7 Hz]; $^{13}C\{^1H\}$ ($CDCl_3$): δ = 188.0 (C1), 152.8 (C7), 132.4 (C5), 127.9 (C3), 125.6 (C2), 125.3 (C4), 121.1 (C6).

2.2.2. Synthesis of $S(C_6H_3CH_2OH)_2O$ (*2*)

1 (1.0 g, 3.9 mmol) was suspended in ethanol (15 mL) and cooled to 0 °C in an ice-bath; then, $Na[BH_4]$ (0.74 g, 19.6 mmol) was added in small portions. The suspension was warmed to room temperature and stirred until the yellow color vanished. The suspension was acidified with HCl to pH 2 and extracted with dichloromethane (2 × 50 mL). The organic layers were dried with Na_2SO_4 and evaporated under reduced pressure; a white solid was obtained. Yield: 97% (1.0 g, 3.8 mmol). M.p.: 135 °C. *Anal.* Calc. for $C_{14}H_{12}O_3S$: C, 64.60; H, 4.65. Found: C, 64.72; H, 4.70%. IR (CsI): ν = 3265(OH), 3154, 3066, 2952, 2923, 2852, 1722, 1586, 1426, 1356, 1291, 1255, 1211, 1056, 1020, 984, 877, 770 cm^{-1}. NMR: ^1H ($CDCl_3$) δ = 7.01 m [2H, H-3, H-5,], 6.91 t [1H, H-4, $^3J_{H3-H4}$ = 7.5, $^3J_{H4-H5}$ = 7.5 Hz], 4.63 s [2H, H-1], 3.60 s [1H, OH]; $^{13}C\{^1H\}$ ($CDCl_3$): δ = 150.3 (C7), 129.0 (C2), 128.7 (C5), 126.7 (C3), 124.4 (C4), 120.1 (C6), 60.8 (C1).

2.2.3. Synthesis of $S(C_6H_3CH_2Br)_2O$ (*3*)

Aqueous HBr (1.7 mL, 15.0 mmol) was added to a solution of **2** (1.0 g, 3.8 mmol) dissolved in toluene (15 mL); the solution was refluxed for 24 h. After the reaction, the organic layers were extracted with chloroform (2 × 50 mL) and dried with Na_2SO_4. After evaporation to dryness, a white solid was obtained. Yield: 92% (1.38 g, 3.6 mmol). M.p.: 174 °C. *Anal.* Calc. for $C_{14}H_{10}Br_2OS$: C, 43.55; H, 2.61. Found: C, 43.98; H, 2.62%. IR (CsI): ν = 2965, 2857,

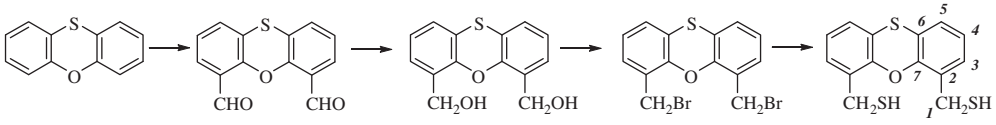

1 2 3 4

Scheme 2. Linear synthesis of dithiol **4**.

1919, 1772, 1713, 1583, 1445, 1430, 1289, 1268, 1229, 1202, 1076, 912, 776, 726, 665, 606, 553, 483 cm^{-1}. NMR: ^1H ($CDCl_3$) δ = 7.10 dd [1H, H-3, $^3J_{H3-H4}$ = 7.5, $^4J_{H3-H5}$ = 1.8 Hz], 6.97 dd [1H, H-5, $^3J_{H4-H5}$ = 7.7, $^4J_{H3-H5}$ = 1.8 Hz], 6.92 dd [1H, H-4, $^3J_{H3-H4}$ = 7.5, $^3J_{H4-H5}$ = 7.7 Hz], 4.67 s [2H, H-1]; $^{13}C\{^1H\}$ ($CDCl_3$): δ = 149.3 (C7), 129.3 (C3), 127.3 (C5), 127.0 (C2), 124.7 (C4), 120.1 (C6), 27.8 (C1).

2.2.4. Synthesis of $S(C_6H_3CH_2SH)_2O$ (**4**)

Thiourea (0.94 g, 12.3 mmol) was added to a solution of **3** (1.60 g, 4.1 mmol) in ethanol (30 mL); the mixture was refluxed for 24 h. An aqueous solution of potassium hydroxide (1.40 g, 25 mmol) was then added to the warm mixture and refluxed for four hours and allowed to reach room temperature. The mixture was acidified with HCl to pH 2 and extracted with chloroform (2 × 50 mL); the organic layers were dried with Na_2SO_4. After evaporation of the organic solvent, a yellow solid was obtained. Yield: 75% (0.90 g, 3.1 mmol). M.p.: 103 °C. *Anal.* Calc. for $C_{14}H_{12}S_3O$: C, 57.50; H, 4.14. Found: C, 58.24; H, 4.18%. IR (CsI): ν = 3162, 3053, 2934, 2553 (SH), 1584, 1461, 1430, 1293, 1265, 1211, 1182, 1078, 970, 889, 780, 735 cm^{-1}. NMR: ^1H ($CDCl_3$) δ = 7.04 dd [1H, H-3, $^3J_{H3-H4}$ = 6.6, $^4J_{H3-H5}$ = 2.6 Hz], 6.90 m [2H, H-4, H-5,], 3.81 d [2H, H-1, $^3J_{H1-SH}$ = 7.6 Hz], 1.92 t [1H, SH, $^3J_{H1-SH}$ = 7.6 Hz]; $^{13}C\{^1H\}$ ($CDCl_3$): δ = 146.1 (C7), 130.2 (C2), 128.1 (C3), 125.8 (C5), 124.7 (C4), 120.2 (C6), 23.7 (C1).

2.3. General synthesis of the 10-R compounds of formula $[\{S(C_6H_3CH_2S)_2O\}SnR^1R^2]$

A tin compound was added to a solution of **4** and DABCO in dichloromethane; the reaction mixture was stirred for 12 h. After the reaction, the DABCO chlorohydrate was filtered off and the remaining solution was slowly evaporated to dryness to get a solid product.

2.3.1. Synthesis of $[\{S(C_6H_3CH_2S)_2O\}SnPh_2]$ (**5**)

Compound **4** (0.20 g, 0.68 mmol), Ph_2SnCl_2 (0.23 g, 0.67 mmol) and DABCO (0.061 g, 0.54 mmol). Yield: 0.22 g (57%). M.p.: 145 °C. *Anal.* Calc. for $C_{26}H_{20}OS_3Sn$: C, 55.43; H, 3.58. Found: C, 55.52; H, 3.49%. IR (KBr): ν = 3051, 3018, 2984, 2918, 1586, 1455, 1436, 1234, 1217, 1180, 1073, 997, 697 cm^{-1}. NMR: ^{119}Sn ($CDCl_3$): δ = 6.5; ^1H ($CDCl_3$) δ = 7.27 tt [1H, H-11, $^3J_{H10-H11}$ = 8.0, $^4J_{H9-H11}$ = 1.2 Hz], 7.15 m [2H, H-3, H10], 7.08 dd [1H, H-9, $^3J_{H9-H10}$ = 8.8, $^4J_{H9-H11}$ = 1.2 Hz], 6.93 t [1H, H-4, $^3J_{H4-H5}$ = 7.7, $^3J_{H4-H3}$ = 7.7 Hz], 6.67 dd [1H, H-5, $^3J_{H4-H5}$ = 7.7, $^4J_{H3-H5}$ = 1.6 Hz], 4.14 s [1H, H-1, $^3J_{H1-^{119}Sn}$ = 56.6 Hz]; $^{13}C\{^1H\}$ ($CDCl_3$): δ = 147.3 (C7), 138.3 (C8), 135.2 (C9), 130.3 (C2), 129.7 (C11), 128.8 (C10), 128.7 (C3), 125.4 (C4), 124.7 (C5), 119.2 (C6), 25.9 (C1).

2.3.2. Synthesis of $[\{S(C_6H_3CH_2S)_2O\}SnClPh]$ (**6**)

Compound **4** (0.30 g, 1.02 mmol), $PhSnCl_3$ (0.17 mL, 1.02 mmol) and DABCO (0.092 g 0.82 mmol). Yield: 0.19 g (35%). M.p.: 156 °C. *Anal.* Calc. for $C_{20}H_{15}ClOS_3Sn$: C, 46.05; H, 2.9. Found: C, 45.47; H, 2.79%. IR (KBr): ν = 3047, 2955, 2923, 2851, 1585, 1462, 1435, 1234, 1210, 1180, 1068, 914, 692 cm^{-1}. NMR: ^{119}Sn ($CDCl_3$): δ = −16.6; ^1H ($CDCl_3$) δ = 7.39 tt [1H, H-11, $^3J_{H10-H11}$ = 7.6, $^4J_{H9-H11}$ = 1.4 Hz], 7.20 t [2H, H-10, $^3J_{H9-H10}$ = 7.6, $^3J_{H10-H11}$ = 7.6 Hz], 7.11 m [4H, H-9, H-3], 6.98 t [2H, H-4, $^3J_{H3-H4}$ = 7.7, $^3J_{H4-H5}$ = 7.7 Hz], 6.77 dd [2H, H-5, $^3J_{H4-H5}$ = 7.7, $^3J_{H3-H5}$ = 1.6 Hz], 4.45 dd [2H, H-1a, $^2J_{H1a-H1b}$ = 13.5, $^3J_{H1a-^{119}Sn}$ = 39.5 Hz], 3.7 ddd [2H, H-1b, $^2J_{H1b-H1a}$ = 13.5, $^3J_{H1b-^{119}Sn}$ = 136.2, $^3J_{H1b-^{117}Sn}$ = 130.3 Hz]; $^{13}C\{^1H\}$ ($CDCl_3$): δ = 146.1 (C7), 141.1 (C8), 133.3 (C9), 130.9 (C2), 130.5 (C11), 129.3 (C10), 127.9 (C3), 125.8 (C4), 125.7 (C5), 119.8 (C6), 28.1 (C1).

2.3.3. Synthesis of $[\{S(C_6H_3CH_2S)_2O\}SnCl(n\text{-}Bu)]$ (**7**)

Compound **4** (0.30 g, 1.02 mmol), $^nBuSnCl_3$ (0.17 mL, 1.02 mmol) and DABCO (0.092 g, 0.82 mmol). Yield: 0.45 g (87%). M.p.: 120 °C. *Anal.* Calc. for $C_{18}H_{19}ClOS_3Sn$: C, 43.09; H, 3.82. Found: C, 43.46; H, 3.66%. IR (KBr): ν = 3054, 2926, 2854, 1712, 1459, 1435, 1232, 1209, 1176, 1076, 705 cm^{-1}. NMR: ^{119}Sn ($CDCl_3$): δ = 28.0; ^1H ($CDCl_3$) δ = 7.13 m [2H, H-3], 7.09 m [4H, H-4, H-5], 4.45 d [2H, H-1a, $^2J_{H1a-H1b}$ = 13.5, $^3J_{H1a-^{119}Sn}$ = 35.6 Hz], 3.70 d [2H, H-1b, $^2J_{H1b-H1a}$ = 13.5, $^3J_{H1b-^{119}Sn}$ = 119.1, $^3J_{H1b-^{117}Sn}$ = 114.2 Hz], 1.88 td [2H, H–8, $^3J_{H8-H9}$ = 7.7, $^3J_{H8-^{119}Sn}$ = 64.4 Hz], 1.45 q [2H, H-9, $^3J_{H8-H9}$ = 7.7, $^3J_{H9-H10}$ = 7.3 Hz], 1.23 sx [2H, H-10, $^3J_{H9-H10}$ = 7.3, $^3J_{H10-H11}$ = 7.3 Hz], 0.73 t [3H, H-11, $^3J_{H10-H11}$ = 7.3 Hz]; $^{13}C\{^1H\}$ ($CDCl_3$): δ = 147.3 (C7), 131.8 (C2), 128.3 (C3), 126.3 (C4), 126.3 (C5), 120.3 (C6), 31.6 (C8), 28.4 (C1), 27.6 (C9), 25.7 (C11), 13.5 (C10).

2.3.4. Synthesis of $[\{S(C_6H_3CH_2S)_2O\}SnCl_2]$ (**8**)

Compound **4** (0.20 g, 0.68 mmol), $SnCl_4$ (0.08 mL, 0.68 mmol) and DABCO (0.061 g, 0.54 mmol). Yield: 0.24 g (74%). M.p.: 146 °C. *Anal.* Calc. for $C_{14}H_{10}Cl_2OS_3Sn$: C, 35.03; H, 2.10. Found: C, 35.05; H, 2.03%. IR (KBr): ν = 2920, 2850, 1585, 1459, 1451, 1435, 1226, 1206, 1172, 1155, 1076, 1058, 967, 675, cm^{-1}. NMR: ^{119}Sn ($CDCl_3$): δ = −97.3; ^1H ($CDCl_3$) δ = 7.10 m [3H, H-3, H-4, H-5], 4.19 s [1H, H-1, $^3J_{H1b-^{119}Sn}$ = 137.6, $^3J_{H1b-^{117}Sn}$ = 131.8 Hz]; $^{13}C\{^1H\}$ ($CDCl_3$): δ = 145.8 (C7), 129.3 (C2), 127.6 (C3), 126.9 (C4), 126.2 (C5), 120.8 (C6), 29.4 (C1, $^2J_{C1-^{119}Sn}$ = 31.9 Hz).

2.4. Synthesis of the 8-R compounds of formula $[\{S(C_6H_3S)_2O\}SnR^1R^2]$

2.4.1. Synthesis of $[\{S(C_6H_3S)_2O\}SnPh_2]$ (**10**)

Compound **9** (0.23 g 0.87 mmol) was dissolved in 25 mL of dry chloroform at room temperature. DABCO (0.13 g, 1.16 mmol) was added and the mixture was stirred for 15 min. Ph_2SnCl_2, (0.40 g, 1.16 mmol) was added to the above mixture and refluxed overnight; during this time the mixture acquired clear yellow coloration. The hot mixture was filtered producing an oily compound that was dissolved in chloroform. The chloroform solution was slowly evaporated giving a yellow solid. Yield: 0.32 g (68%). M.p.: 120 °C. *Anal.* Calc. for $C_{16}H_{15}ClOS_3Sn$: C, 53.85; H, 3.01. Found: C, 53.75; H, 2.99%. IR (KBr): ν = 3048, 2917, 2849, 1629, 1582, 1407, 1229, 1067, 835, 769, 724, 693, 442 cm^{-1}. NMR: ^{119}Sn ($CDCl_3$): δ = −11.7; ^1H ($CDCl_3$): δ = 7.50 m [4H, H-9], 7.40 dd [2H, H-3, $^3J_{H3-H4}$ = 7.8, $^4J_{H3-H5}$ = 1.3 Hz], 7.34 m [6H, H-10, H-11], 6.95 t [2H, H-4, $^3J_{H3-H4}$ = 7.8, $^3J_{H4-H5}$ = 7.8 Hz], 7.86 dd [2H, H-5, $^3J_{H4-H5}$ = 7.8, $^4J_{H3-H5}$ = 1.3 Hz]; $^{13}C\{^1H\}$ ($CDCl_3$): δ = 148.0 (C7), 139.5 (C8, $^1J_{C8-Sn}$ = 632, 604 Hz), 135.4 (C9, $^2J_{C9-Sn}$ = 50 Hz), 130.6 (C3, $^3J_{C8-Sn}$ = 28 Hz), 130.4 (C11, $^4J_{C11-Sn\,=\,14}$ Hz), 129.2 (C10, $^3J_{C8-Sn}$ = 68 Hz), 125.4 (C4), 124.8 (C2, $^2J_{C8-Sn}$ = 24 Hz), 123.9 (C5), 121.4 (C6).

2.4.2. Synthesis of $[\{S(C_6H_3S)_2O\}SnCl(n\text{-}Bu)]$ (**11**)

Compound **11** was prepared in a similar approach to **10** except for the addition of DABCO.

Compound **9** (0.75 g, 2.84 mmol) and $BuSnCl_3$ (0.5 mL, 2.85 mmol). Brown solid. Yield: 0.66 g (50%). M.p.: 85 °C. *Anal.* Calc. for $C_{16}H_{15}ClOS_3Sn$: C, 40.57; H, 3.19. Found: C, 40.35; H, 3.15%. IR (KBr): ν = 3062, 2956, 2920, 2846, 1653, 1561, 1440, 1408, 1239, 913, 871, 839, 764, 704 cm^{-1}. NMR: ^{119}Sn ($CDCl_3$): δ = −15.2; ^1H ($CDCl_3$): δ = 7.29 dd [2H, H-3, $^3J_{H3-H4}$ = 7.8, $^4J_{H3-H5}$ = 1.6 Hz], 7.02 t [2H, H-4, $^3J_{H3-H4}$ = 7.8, $^3J_{H4-H5}$ = 7.8 Hz], 6.96 dd [2H, H-5, $^3J_{H4-H5}$ = 7.8, $^4J_{H3-H5}$ = 1.6 Hz], 2.04 dd [2H, H-8, $^3J_{H8-H9}$ = 8.2, $^3J_{H8-H9}$ = 7.6 Hz], 1.74 q [2H, H-9, $^3J_{H8-H9}$ = 7.7 Hz], 1.39 sx [2H, H-10, $^3J_{H9-H10}$ = 7.4 Hz], 0.85 t [3H, H-11, $^3J_{H10-H11}$ = 7.4 Hz]; $^{13}C\{^1H\}$ ($CDCl_3$): δ = 147.5 (C7, $^3J_{C7-Sn}$ = 14 Hz), 129.5 (C3, $^3J_{C3-Sn}$ = 44 Hz), 126.7 (C4), 125.5 (C2), 124.0 (C5), 123.4 (C6),

31.5 (C8), 27.2 (C9, $^2J_{C9\text{-}Sn}$ = 48 Hz), 25.6 (C10, $^3J_{C10\text{-}Sn}$ = 34 Hz), 13.6 (C11).

*2.4.3. Synthesis of [{S(C$_6$H$_3$S)$_2$O}SnCl$_2$] (**12**)*

$SnCl_4$ (0.5 mL, 4.27 mmol) was dissolved in dry toluene (20 mL) at −78 °C. The solution was stirred for 30 min, then **9** (1.13 g, 4.27 mmol) in dry toluene (20 mL) was added with a syringe. The solution was kept at 5 °C overnight. The mixture was then filtered and the toluene fraction was slowly evaporated. A yellow solid was obtained. Yield: 0.78 g (41%). M.p.: 54 °C. *Anal.* Calc. for $C_{12}H_6Cl_2OS_3Sn$: C, 31.89; H, 1.34. Found: C, 31.53; H, 1.99%. IR (KBr): ν = 3058, 2913, 2849, 1610, 1589, 1458, 1440, 1416, 1224, 877, 839, 764, 704 cm^{-1}. NMR: ^{119}Sn ($CDCl_3$): δ = −134.9; ^{1}H ($CDCl_3$): δ = 7.32 dd [2H, H-3, $^3J_{H3-H4}$ = 7.9, $^4J_{H3-H5}$ = 1.4 Hz], 7.11 t [2H, H-4, $^3J_{H3-H4}$ = 7.9 Hz, $^3J_{H4-H5}$ = 7.9 Hz], 7.03 dd [2H, H-5, $^3J_{H4-H5}$ = 7.9, $^4J_{H3-H5}$ = 1.4 Hz]; ^{13}C{^{1}H} ($CDCl_3$): δ = 144.8 (C7), 129.0 (C3), 126.7 (C4), 124.9 (C5), 122.5 (C2), 121.4 (C6).

2.5. X-ray Crystallography and structure solution

Suitable single crystals of the compounds **5**, **7**, **8**, **10**, and **11** were grown by slow evaporation from a chloroform solution. X-ray diffraction data for **7** and **8** were collected at 141 K on an Oxford Diffraction Gemini CCD diffractometer with graphite-monochromated Mo Kα radiation (λ = 0.71073 Å) was used. Data were integrated, scaled, sorted, and averaged using the CRYSALIS software package [14]. An analytical numeric absorption correction using a multifaceted crystal model was applied by using the CRYSALIS Software. Data of compound **5** were collected on a Bruker SMART X2S benchtop crystallographic system with monochromated (doubly curved silicon crystal) Mo Kα radiation (0.71073 Å) from a sealed microfocus tube at 300 K. Data for **10** and **11** were collected at room temperature on a CCD SMART 6000 diffractometer through the use of Mo Kα radiation (λ = 0.71073 Å, graphite monochromator). Data of **5**, **10**, and **11** were integrated, scaled, sorted, and averaged using the SMART software package. An empirical absorption correction based on the multiple measurement of equivalent reflections was applied with the program SADABS [15].

All the structures were solved by direct methods, using SHELXTL NT Version 5.10 and refined by full-matrix least squares against F^2 [16]. The displacement parameters of non-hydrogen atoms were anisotropically refined. The positions of the hydrogen atoms were kept fixed with a common isotropic displacement parameter. Selected crystallographic data are given in Table 1.

2.6. Theoretical study

To study the conformational preference, a conformational search was performed by molecular mechanics force field (MMFF) in the selected compounds **5**, **7**, **8**, **10**, **11**, and **12**; the SPARTAN 08 program [17] employing the Monte–Carlo algorithm was used. The conformations were generated by systematic change of torsion angles of the freely rotating bonds. The low-energy conformers were preselected in range the 10 kcal/mol. The most stable conformers of these selected compounds were subjected to quantum chemical geometrical optimization using several functionals (LSDA, BLYP, B3LYP, and M06) using the DGDZVP or TZVP basis set in gaseous phase for all the atoms except Sn, for which a relativistic effect core potential RECP was used [18,19]. These calculations were denoted as functional/TZVP+RECP(Sn). For the total optimization in chloroform as solvent, we employed the integral equation formalism polarizable continuum model (IEFPCM) [20,21]. For all the systems, the lowest state energy from the second derivative calculation was used to analyze the stability of the systems. The nature of the chemical bonding was analyzed in terms of the topology of the electronic density [$\rho(r)$]. All calculations were performed with the GAUSSIAN 09 program [22]. The ground-state wave-function was used for "atoms in molecules" (AIM) calculation [23] to determine bond critical points (BCPs) and ring critical points (RCPs); the results were analyzed in terms of electron densities (ρ) ellipticity (ε), energy density [$E_d(r)$] and their Laplacians ($L = -1/4\nabla^2\rho$). The Bader theory is applied in the AIM 2000 program [24].

3. Results and discussion

3.1. Synthesis of the dithioligands S(C$_6$H$_3$CH$_2$SH)$_2$O (4) and S(C$_6$H$_3$SH)$_2$O (**9**)

Ditihioligand **4** was prepared by linear synthesis from phenoxathiin by taking advantage of the regioselectivity of the dilithiation reaction in the *ortho*-position with respect to the oxygen atom; the dialdehyde (**1**), diol (**2**), and dibromo (**3**) intermediate compounds were isolated and structurally characterized (See Section 2 and Scheme 2 for details). Compound **9** was prepared via a one-pot four-step reaction from phenoxathiin [13].

3.2. Synthesis of the tin compounds ***5*–*8*** and ***10*–*12***

The reaction of **4** or **9** with the corresponding chlorotin compound dissolved in dry dichloromethane or chloroform in the presence of the deprotonating reagent DABCO yielded the corresponding compounds **5**–**8** and **10** with moderate yields. **11** was similarly prepared but without DABCO. The treatment of **9** with $SnCl_4$ in dry toluene at −78 °C afforded the dichlorotin compound **12**. The general reactions are shown in the Scheme 3. All compounds are air-stable. **6**, **8**, and **12** are slightly soluble in chloroform, methylene chloride and benzene; the remaining compounds are quite soluble in these solvents. All tin compounds are insoluble in *n*-hexane, pentane, methanol, and 2-propanol.

3.3. NMR spectra

NMR spectra of all the compounds were recorded in $CDCl_3$ solutions at room temperature and the chemical shifts are relative to TMS. Assignment of all compounds was performed by ^{1}H, ^{13}C and ^{119}Sn experiments; the signals were corroborated for some selected compounds by two dimensional ^{1}H–^{1}H gCOSY, ^{1}H–^{13}C gHMBCAD, and ^{1}H–^{13}C HSQC experiments. In solution the two (S{C$_6$H$_3$(CH$_2$)$_n$S}O)Sn (n = 1, 0) halves are equivalent.

^{1}H NMR spectra of compounds **1**–**6** and **10**–**12** showed three signals in an ABC pattern for the protons of the phenoxathiin rings; **7** and **8** displayed a higher order spectra for the aromatic protons of these rings.

For **4**, the signal for the –S<u>H</u> proton at 3.81 ppm is displayed as a triplet because of the coupling with the C<u>H</u>$_2$-S protons resonating at 1.92 ppm; for **9**, the –S<u>H</u> is displayed as a single signal at 4.05 ppm. These signals and the couplings vanished when the ligands **4** or **9** were coordinated with the appropriate starting material of tin.

The ^{1}H NMR spectra of the compounds in the ***10*-*R*** series deserve a more thorough discussion. In the case of compounds **5** and **8**, the C<u>H</u>$_2$-S-Sn protons are observed as single signals, while for the compounds **6** and **7** these protons are displayed as an AB system, with geminal coupling constants of 13.5 and 13.6 Hz, respectively; all ***10*-*R*** compounds displayed these signals assigned to the methylenic protons with satellites that are caused by spin–spin interactions with the tin isotopes $^{117/119}$Sn (Fig. 1). In **6** and **7**, the most shifted signals towards higher frequencies with respect to the free ligand **4** were assigned to the *endo* protons, with a variation of the chemical shift, $\Delta\delta$, of 0.64 ppm; these *endo* and *exo* protons were also

Table 1
Selected crystallographic data for compounds **5**, **7**, **8**, **10**, and **11**.

Compound	**5**	**7**	**8**	**10**	**11**
Empirical formula	$C_{26}H_{20}OS_3Sn$	$C_{18}H_{19}ClOS_3Sn$	$C_{14}H_{10}Cl_2OS_3Sn$	$C_{24}H_{16}OS_3Sn$	$C_{16}H_{15}ClOS_3Sn$
Molecular weight (g/mol)	563.29	501.65	479.99	535.24	473.60
Crystal size (mm)	0.60 × 0.60 × 0.50	0.38 × 0.26 × 0.10	0.59 × 0.52 × 0.23	0.27 × 0.21 × 0.09	0.40 × 0.40 × 0.30
Color	colorless	colorless	yellow	colorless	colorless
Crystal System	monoclinic	monoclinic	monoclinic	triclinic	triclinic
Space group	$P2_1/n$	$P2_1/c$	$P2_1/n$	$P\bar{1}$	$P\bar{1}$
ρ_{calc} (mg m^{-3})	1.596	1.790	1.974	1.606	1.741
Z	4	4	4	2	2
a (Å)	7.6372(8)	9.2062(2)	8.4276(3)	9.1578(13	7.4311(8)
b (Å)	20.694(3)	15.4747(4)	14.2829(3)	10.5411(15)	8.3387(9)
c (Å)	14.8330(19)	13.0972(3)	13.8622(4)	12.3659(17)	14.8568(16)
α (°)	90	90	90	77.378(3)	85.267(2)
β (°)	90.056(4)	94.090(2)	104.585(3)	71.886(3)	85.119(2)
γ (°)	90	90	90	85.748(3)	80.822(2)
V (Å^3)	2344.3(5)	1861.12(9)	1614.84(8)	1107.1(3)	903.30(17)
μ (mm^{-1})	1.374	1.856	2.294	1.450	1.906
F(000)	1128	1000	936	532	468
θ range (°)	0.98–25.07	3.39–26.06	3.53–26.05	1.77–26.09	1.38–26.08
Completeness to θ	99.1	99.8	99.7	99.8	99.1
Goodness of fit	1.070	1.032	1.080	0.984	1.080
Reflections collected	22729	13675	10939	13764	6042
Unique reflections, (R_{int})	4129	3670	3190	4383	3563
R_1, wR_2 [$I > 2\sigma(I)$]	0.0429, 0.1167	0.0187, 0.0449	0.0301, 0.0769	0.0475, 0.0870	0.0261, 0.0639
R_1, wR_2 (all data)	0.0499, 0.1232	0.0242, 0.0461	0.0358, 0.0794	0.0947, 0.1042	0.0296, 0.0658
Large residuals (e Å^{-3})	1.061 and −0.859	0.373 and −0.293	0.644 and −0.912	0.620 and −0.314	0.297 and −0.355

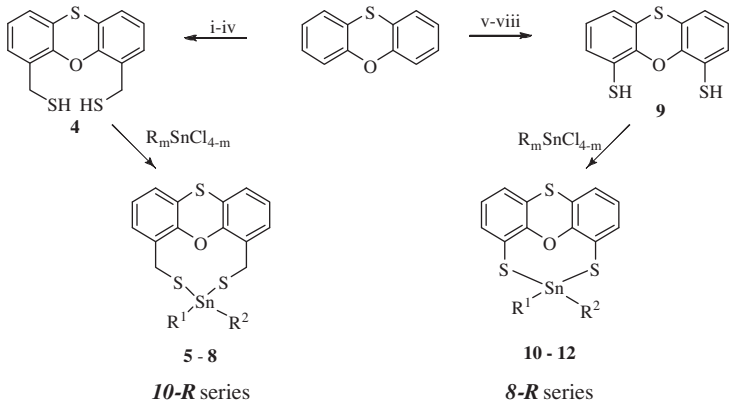

series		m	R^1	R^2	$^{119}Sn\{^1H\}$ NMR (ppm)
10-R	**5**	2	Ph	Ph	6.5
	6	1	Cl	Ph	−16.6
	7	1	Cl	*n*-Bu	28.0
	8	0	Cl	Cl	−97.3
8-R	**10**	2	Ph	Ph	−11.7
	11	1	Cl	*n*-Bu	−15.2
	12	0	Cl	Cl	−134.9

Scheme 3. Synthesis of compounds **4–12**. (i) *n*-BuLi/TMEDA/DMF/hexane; (ii) Na[BH_4]/ethanol; (iii) HBr/toluene; (iv) Thiourea/KOH/H^+/ethanol; (v) *n*-BuLi/TMEDA/THF; (vi) Elemental sulfur; (vii) Li[AlH_4]; (viii) HCl/H_2O.

observed in the correspondent molecular structures studied by X-ray single crystal diffraction experiments (vide infra). The *exo* protons were observed at low frequencies with $\Delta\delta$ 0.11 ppm; their assignment was confirmed with a ^1H–^1H noesy experiment. For example, for **7**, a ^1H–^1H correlation was observed for the signals at 3.70 and 7.13 ppm, where this last frequency is assigned to the proton *ortho* to the CH_2-S-Sn fragment. For compounds **5** and **8** the C$\underline{H}_2$-S-Sn protons showed $^3J(^1H–^{117/119}Sn)$ coupling constants of 56.6 and 131.8/137.6 Hz, respectively. On the other hand, these protons in the compounds **6** and **7** displayed two different $^3J(^1H–^{117/119}Sn)$ couplings: for the *endo* protons were observed couplings of 39.5 Hz and 35.6 Hz for **6** and **7**, respectively, while for the *exo* protons there were observed two couplings of 130.3/136.2 Hz for **6** and 114.2/119.1 Hz for **7**. The large values of the couplings found for the *exo* protons in **6**, **7** and for the H1 proton in **8** are in good agreement with couplings reported in some organotin compounds with different substituents at the tin atom containing weak intramolecular ***D*** · · · Sn interactions in solution [25].

The ^{119}Sn NMR spectra for compounds **5**–**12** in the poor-coordinating $CDCl_3$ solvent displayed a single signal indicating the presence in solution of a unique tin compound (data tabulated in Scheme 3). The ^{119}Sn resonances for the ***8-R*** series are generally

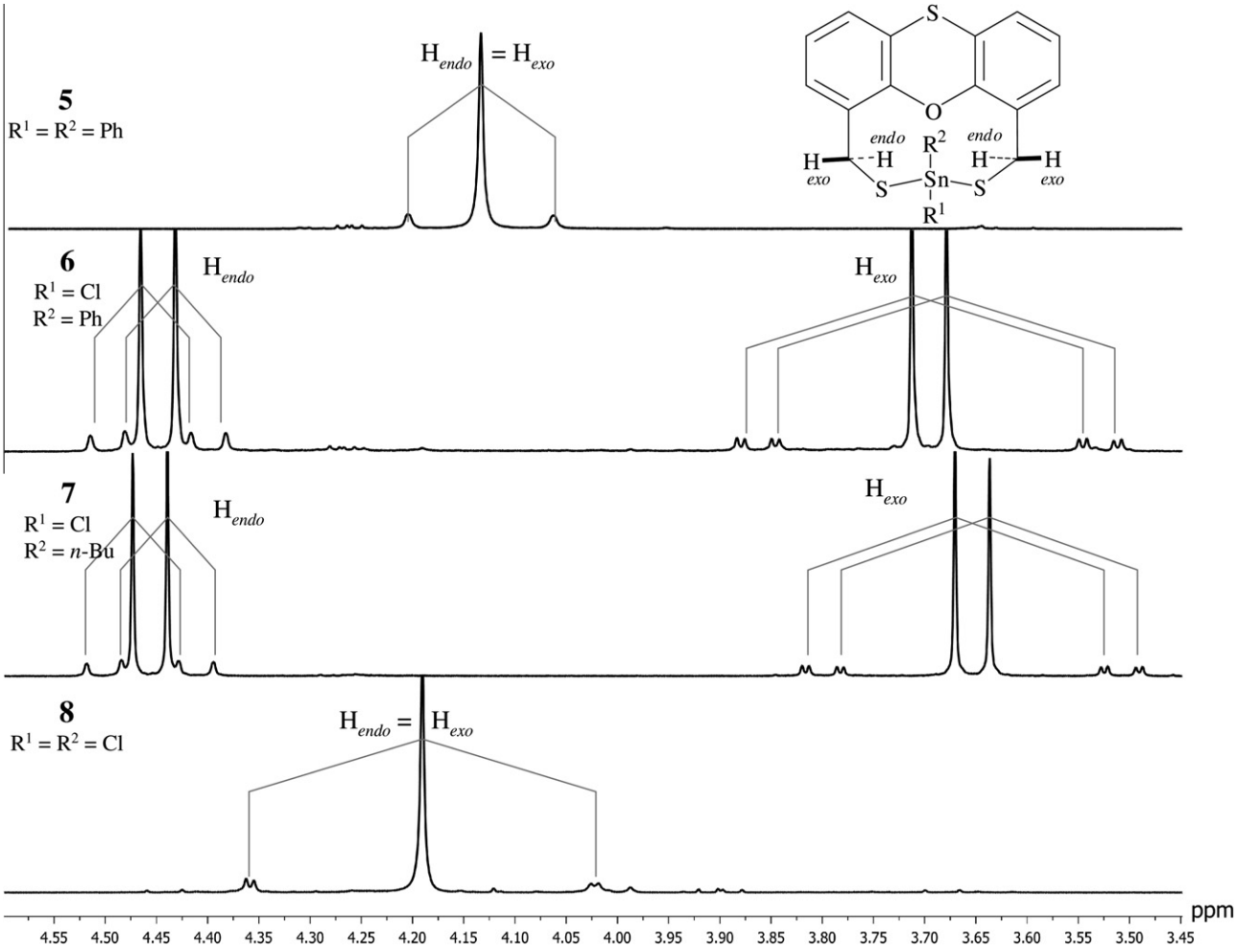

Fig. 1. ^{1}H NMR spectra at 400 MHz at 25 °C in $CDCl_3$ of compounds **5**–**8** in the region of the methylenic protons for the $C\underline{H}_2$-S-Sn fragment showing the satellites with the tin isotopes $^{117/119}$Sn. $^{2}J(^{1}H–^{1}H)$/Hz = 13.5 (**6**); 13.6 (**7**). $^{3}J(^{1}H–^{117/119}Sn)$/Hz = 56.6 (**5**); 39.5 and 130.3/136.2 (**6**); 35.6 and 114.2/119.1 (7); 131.8/137.6 (**8**).

shifted to lower frequencies with respect to the ***10*-*R*** series, with the dichloro compounds **8** and **12** displaying the highest shifting. In several studies, it has been stated that the ^{119}Sn chemical shifts move to lower frequencies as the coordination number increases [26–28]; thus, according to the reported ranges, just **8** and **12** display a coordination number of five in solution. The penta-coordination is explained by the covalent bonding of the tin atom with the electronegative chloro groups and the tridentate ligand $(S\{C_6H_3(CH_2)_nS\}_2O)^{2-}$ (n = 1, 0), where a O···Sn coordination is present because the enhancement of the Lewis acidity on the tin atom. For the remaining compounds, the ^{119}Sn chemical shifts at higher frequencies indicate the presence in solution of tetra-coordinate tin compounds, i.e., the O···Sn interaction is weak.

3.4. Description of the structures of *5*, *7*, *8* (*10*-*R* series), *10*, and *11* (*8*-*R* series) compounds

The crystal structures of the compounds were determined by single-crystal X-ray diffraction analyses. The molecular drawings of **5**, **7**, **8** (***10*-*R***** series), **10** and **11** (***8*-*R***** series) are depicted in Figs. 2–6 and selected bond lengths, angles and some relevant structural features are given in Table 2.

In spite of the structural differences, some general features are common for the ***10*-*R*** and ***8*-*R*** series with the general formula $[(S\{C_6H_3(CH_2)_nS\}_2O)SnR^1R^2]$ (n = 1, 0). For example, all tin-carbon bond distances agree very well with the corresponding sum of covalent radii [29]. Likewise, the Sn–S(thiolate-like) distances also agree with those reported for eight-membered heterocycles and several other compounds with tin–sulfur bonds [9]. In addition, the tricyclic phenoxathiin moiety present in the compounds compels a mirror-related conformation of the ten- and eight-membered central ring, with angles between the aromatic rings ranging

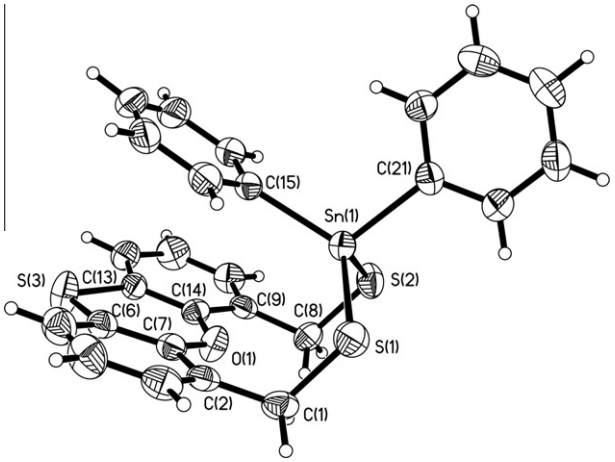

Fig. 2. Molecular structure of $[\{S(C_6H_3CH_2S)_2O\}SnPh_2]$ (**5**).

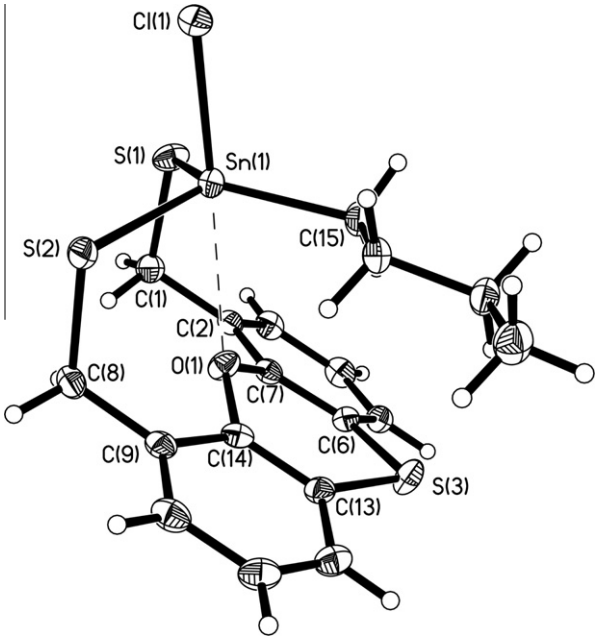

Fig. 3. Molecular structure of [{S($C_6H_3CH_2S)_2$O}SnCl(*n*-Bu)] (**7**).

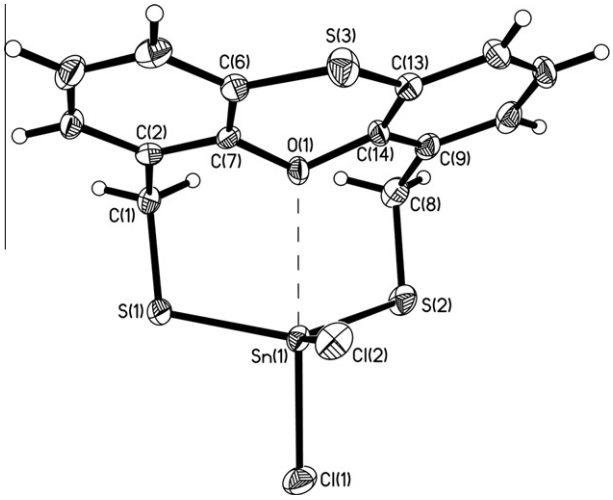

Fig. 4. Molecular structure of [{S($C_6H_3CH_2S)_2$O}$SnCl_2$] (**8**).

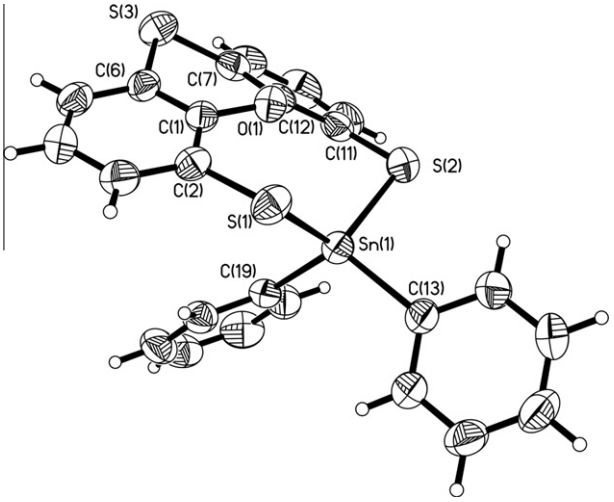

Fig. 5. Molecular structure of [{S($C_6H_3S)_2$O}$SnPh_2$] (**10**).

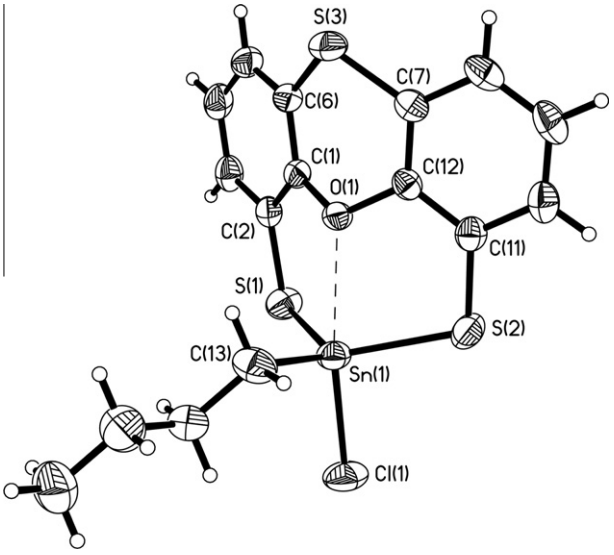

Fig. 6. Molecular structure of [{S($C_6H_3S)_2$O}SnCl(*n*-Bu)] (**11**).

from 170 to 142°. It is noteworthy that in all compounds there is observed an O···Sn transannular distance shorter than the sum of the van der Waals radii [3.281(4), (**5**); 2.7560(13), (**7**); 2.7426(19), (**8**); 3.002(3), (**10**); 2.4720(16) Å (**11**); Σr_{vdW} (Sn, O) = 3.69 Å] [30]; this short distance is usually related to the presence of secondary bonding [29].

From the analysis of the bond angles around the tin atom, it is possible to see that the O···Sn interaction influences the tin local geometry along the path from tetrahedral to trigonal bipyramidal (tbp). In order to evaluate this displacement of geometry (tbp%), the difference between the sum of the equatorial and axial angles [$\Delta = \Sigma(\theta)_{equatorial} - \Sigma(\theta)_{axial}$] was used [31]; the evaluation of the magnitude of the O···Sn interaction was carried out from the Pauling-type Bond Order (BO) based on interatomic distances [32,33]. The data are listed in Table 2. The local tin geometry in the chloro compounds **7**, **8** and **11** can be described as distorted tbp, whereas in the diphenyl compounds **5** and **10** the geometry is best described as tetrahedral. In general, the BO becomes smaller for the compounds in the ***8*-*R*** series because of the smaller ring size; within each series, the BO is larger as the number of the chloro groups increases, i.e., the compound **8** displays the larger BO because of the higher Lewis acidity of the Sn atom.

The conformation of the compounds deserves a detailed discussion; firstly, in compounds **5**, **7** and **8** (***10*-*R*** series) the conformation of the [{S($C_6H_3CH_2S)_2$O}Sn] tetracyclic moiety is very similar, with the methylenic hydrogen atoms of the CH_2-S-Sn fragment located on *endo* and *exo* positions, a situation similar to that observed in the NMR studies in solution (vide supra). The conformation of the eight-membered central rings in this series can be described as boat, despite the different pendant ligands. On the other hand, the conformation of the [{S($C_6H_3S)_2$O}Sn] moiety in compounds **10** and **11** (***8*-*R*** series) is totally different; the conformation of the central ring in **10** can be described as boat-chair meanwhile in **11** is described as boat-boat, very similar to what is observed in the germanium and lead analog compounds [10,13]. Secondly, with respect to the ligands attached to the tin atom, the organic group is stacked directly above the aromatic system of the phenoxathiin moiety in the organotin compounds **5** and

Table 2
Selected bond lengths (Å), angles (°), and structural parameters for heterocyclic compounds **5**, **7**, **8** (***10*-*R*** series), **10** and **11** (***8*-*R*** series) with general formula $[(S\{C_6H_3(CH_2)_nS\}_2O)SnR^1R^2]$ (n = 1, 0).

		10*-*R		***8*-*R***	
	5	**7**	**8**	**10**	**11**
n	1	1	1	0	0
R^1	Ph	Cl	Cl	Ph	Cl
R^2	Ph	*n*-Bu	Cl	Ph	*n*-Bu
O···Sn	3.281(4)	2.7560(13)	2.7426(19)	3.002(3)	2.4720(16)
Sn–S1	2.4107(18)	2.4108(5)	2.3617(8)	2.4267(16)	2.4131(7)
Sn–S2	2.4144(17)	2.4032(5)	2.3621(9)	2.4276(16)	2.4139(8)
Sn–R^{1a}	2.145(5)	2.3645(5)	2.3399(8)	2.120(5)	2.3685(8)
Sn–R^{2a}	2.146(5)	2.1331(19)	2.3360(8)	2.128(5)	2.127(3)
O···Sn–R^{1a}	178.94(15)	175.77(3)	175.94(5)	150.42(16)	166.51(5)
O···Sn–R^{2a}	70.89(16)	77.76(6)	76.72(5)	92.55(15)	87.03(9)
S1–Sn–S2	115.09(6)	115.87(2)	123.61(3)	119.10(6)	116.31(3)
R^1–Sn–R^{2a}	108.9(2)	102.49(6)	99.26(3)	117.0(2)	106.29(8)
S1–Sn–R^{1a}	102.73(15)	100.673(18)	99.03(3)	103.98(16)	95.22(3)
S1–Sn–R^{2a}	114.14(15)	119.45(6)	113.96(3)	108.14(16)	115.89(10)
S2–Sn–R^{1a}	100.97(15)	94.668(19)	98.95(3)	101.69(16)	97.94(3)
S2–Sn–R^{2a}	113.33(16)	116.91(5)	115.07(3)	107.38(15)	119.13(9)
C–O–C	122.7(4)	120.47(15)	120.0(2)	117.6(4)	116.99(17)
C–S3–C	101.4(2)	99.95(9)	99.62(16)	98.4(3)	98.64(11)
FA[b]	170.1	161.9	159.3	145.0	142.3
tbp%[c]	33.3	60.4	61.6	13.3	57.6
BO[d]	0.0246	0.1353	0.1414	0.0609	0.3403

[a] R^1 and R^2 mean an atom directly attached to the central tin atom (v.gr. carbon in the phenyl group).
[b] Folding angle between the two C_6 aromatic planar rings of the phenoxathiin moiety.
[c] tbp%: displacement from tetrahedral to trigonal bipyramidal local geometry at Sn; calculation according to the method of differences in angles $\Delta = \Sigma(\theta)_{equatorial} - \Sigma(\theta)_{axial}$, see text.
[d] Pauling-type bond order: $BO = 10^{-(1.41\Delta d)}$, where $\Delta d = (O\cdots Sn)_{exp} - \Sigma r_{cov}$, according to the covalent radii sum Σr_{cov}(Sn, O) = 2.14 Å.

7 (***10*-*R*** series), with distances calculated from the centroid of the O1–C7–C6–S3–C13–C14 six-membered ring to the C15 atom smaller than 3.393 Å. By contrast, in the more rigid compounds **10** and **11** (***8*-*R*** series) the organic ligands are far from the phenoxathiin moiety.

A subtle difference in the conformations is the dihedral angle between the rings of the phenoxathiin moiety. In the case of **5** the $S(C_6H_3S)_2O$ moiety is concave, with the phenyl group inside the concavity and an O···Sn distance of 3.281(4) Å. For **7** the moiety is convex, with a short O···Sn distance of 2.7560(13) Å. The same convexity is observed in the dichloro compound with the shortest O···Sn distance in the ***10*-*R*** series. With respect to the ***8*-*R*** series, a similar situation is observed; for **10** the phenyl group is inside the concavity whereas the *n*-butyl group is outside in the compound **11**.

3.5. Theoretical studies of *5*, *7*, *8* (*10*-*R*), *10*, *11*, and *12* (*8*-*R*) compounds

The conformational diversity of the compounds in the ***8*-*R*** and ***10*-*R*** series has been posed by the results of the NMR and single crystal X-ray studies. For example, the most dramatic difference in the conformation of the eight-membered central ring in the ***8*-*R*** series is displayed by the **10** and **11** compounds, where the former adopted a boat-chair conformation with a long transannular O···Sn distance while **11** adopted a boat-boat conformation with a significant O···Sn interaction. Thus, in order to study the conformational preferences and the bonding situation, we performed a molecular mechanics force field (MMFF) conformational search in the selected compounds **5**, **7**, **8**, **10**, **11**, and **12**. For **5**, **8**, **10**, and **12** there were found two conformers while for **7** and **11** were found four (See the Supplementary material, Figs. 1S–6S). A structural optimization was then performed for these conformers by using several functionals (LSDA, BLYP, B3LYP, and M06) and DGDZVP and TZVP basis set in gaseous phase to find out a suitable functional to reproduce the overall structure of the compounds observed in solid state. The results show that the functionals LSDA and M06 reproduce better the molecular structure, matching with the X-ray structures than others functionals (see the Supplementary material, Table 1S). For example, for the conformers of compound **10**, the energy difference is 0.36 kcal/mol for LSDA and 1.55 kcal/mol for M06 with the DGDZVP basis set; the same tendency was observed when the optimization for all the systems was performed with IEFPCM in chloroform as solvent. Moreover, the total optimization of the conformers by LSDA and M06 but using TZVP+RECP(Sn) basis set in the gaseous state as well as in chloroform as solvent also reproduced the X-ray structure (see Table 2S). The results indicated that LSDA and M06 functionals with the DGDZVP or TZVP+RECP(Sn) basis set are more suitable to describe the X-ray structure than any other functional, because the largest energy difference between the conformers was observed when greater basis sets were used. It was also observed that the combination M06/TZVP+RECP(Sn) produced a smaller error than other combinations in the chloroform solvent [(Error calculation = (Experimental data − calculated data)/Experimental data] (See Supplementary material, Table 3S). Thus, the geometrical parameters such as bond lengths and bond angles obtained through M06/TZVP+RECP(Sn) employing IEFPCM in chloroform as solvent were used to explain the molecular structures. The crystal structure of compound **12** was not obtained; however, its theoretical study was carried out for the sake of comparison. The conformations for the compound **7** are showed in the Fig. 7 (see the Supplementary material for the conformations of the other compounds). For all compounds the most stable conformer agreed with that observed in solid state; the relative differences between the two most stable isomers are small. These small differences can explain the NMR data in solution for the compounds **7** and **11** where a coordination number of four was proposed, a different situation with respect to that observed in solid state where these compounds displayed a coordination number of five because of the electronegativity of the chloro group. Selected bond lengths and angles for the optimized structures obtained from M06/

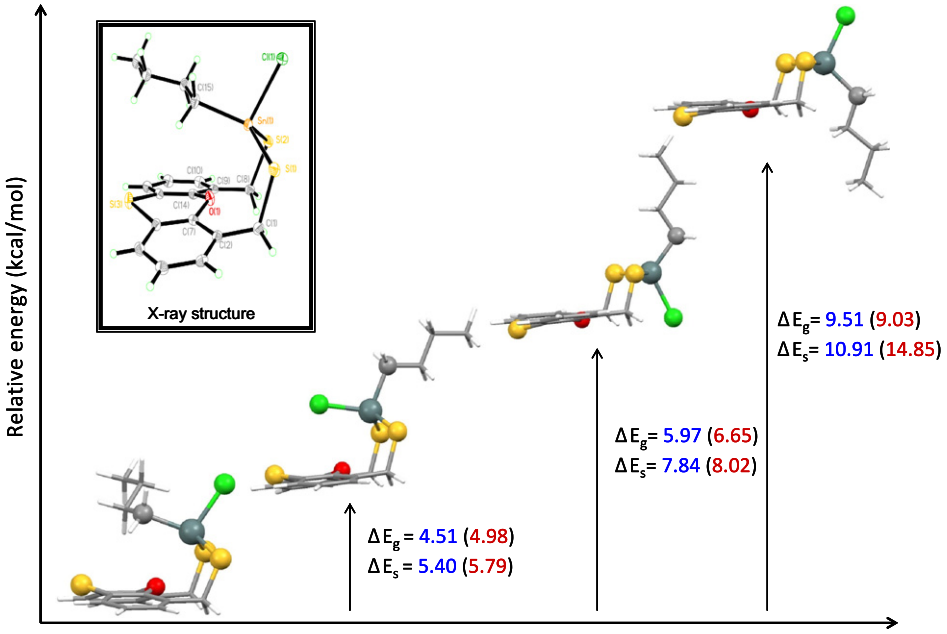

Fig. 7. Conformations of compound **7** in gas phase (g) and in solvent (s); relative energies ΔE for each phase are in kcal/mol (LSDA in blue and M06 in red, both with TZVP+RECP(Sn) basis set).

TZVP+RECP(Sn) employing IEFPCM in chloroform are given in the Table 4S of the supplementary material. The theoretical calculations at the level show that the distances and angles around the Sn atom are in good agreement with the experimental structural data; the O···Sn calculated distances are slightly longer than the experimental ones. In the case of both ***8*-*R*** and ***10*-*R*** series, the folding of the phenoxathiin system as well as the convexity calculated are also in good agreement with the dihedral angles and relative positions of the pendant R ligands observed experimentally.

For the optimized systems of the most stable conformers, the bond critical points of the electron density (BCPs) and the gradient paths were determined. The topological analysis of the electron density is presented in Table 5S and 6S; the molecular graphs for the compounds **5** and **7** are depicted in the Fig. 7S of the Supplementary material. The molecular graphs show that the BCP's are present along with the O···Sn direction. The values of ρ_c for the interaction O···Sn range from 0.007 to 0.044 a.u. and the values of $\nabla^2\rho_c$ are positive; in particular, the ρ_c are the smaller when the two pendant ligands are phenyl groups and they are larger as the number of the chloro groups increases, supporting the experimental data for the oxygen-tin distances observed in solid state by means of the X-ray single crystal diffraction studies.

It is important to note that the L values of all bond critical points connecting Sn with its neighbors are negative, ranging from −0.005 to −0.036 a.u. where the Sn–S and Sn–R bonds have a very important closed shell contribution. In addition, the parameters such as ellipticity (ε) and energy density Ed(r) for Sn and O atoms were also calculated through a Bader's theory point of view (see Supplementary material, Tables 5S and 6S). The results showed that for all cases $\varepsilon > 0$, $\rho(r)$ is small, $\nabla^2\rho(r) > 0$, and Ed(r) > 0; these data suggest that the O···Sn interaction in the complexes corresponds, in fact, to a typical closed-shell (electrostatic) interaction. This situation is consistent with the Hirschfeld charge with a positive value for Sn (0.03–0.13) and a negative value for O (−0.09 to −0.05), indicating that the presence of an ionic type of interaction between Sn and O atoms. The analyses presented above allow us to classify as intramolecular donor-acceptor compounds, in which Sn acts as an acceptor and the oxygen atom as a donor.

4. Conclusion

In order to study the hypercoordination in heterocyclic tin compounds we have synthesized, characterized and studied by theoretical calculations two series of compounds with general formula $[(S\{C_6H_3(CH_2)_nS\}_2O)SnR^1R^2]$ (n = 1, 0). In the solid state, the ***10*-*R*** and ***8*-*R*** chloro compounds **7**, **8**, and **11** displayed a distorted tetrahedral local geometry at the Sn center, whereas the diphenyl compounds **5** and **10** displayed a distorted tetrahedral geometry. In the ***10*-*R*** series, the flexible ligand $\{S(C_6H_3CH_2S)_2O\}^{2-}$ showed coordination modes similar to the $(SnR^1R^2)^{2+}$ fragment with different O···Sn distances depending on the Lewis acidity of the Sn acceptor. On the other hand, the more rigid ligand $\{S(C_6H_3S)_2O\}^{2-}$ present in the ***8*-*R*** series displayed bi- and a tridentate coordination modes toward Sn with different conformations. In general, the distances and Pauling-type bond orders are smaller for the eight-membered compounds when they are compared with the ten-membered analog compounds; however, these larger rings in the ***10*-*R*** series can also form a transannular interaction by adopting an adequate boat conformation. These findings were supported by the conformational study by MMFF and the optimization of the structures with M06/TZVP+RECP(Sn) with calculations in chloroform, and by the topological analysis, where the bonds around the tin atom have an important ionic contribution.

Acknowledgments

DMO and EJG fully acknowledge CONACYT for his fellowship. This research was supported by CONACyT (Project 83157).

Appendix A. Supplementary data

CCDC 862761, 862762, 862763, 862759, and 862760 contain the supplementary crystallographic data for **5**, **7**, **8**, **10**, and **11**. These data can be obtained free of charge via http://www.ccdc.cam.ac.uk/conts/retrieving.html, or from the Cambridge Crystallographic Data Centre, 12 Union Road, Cambridge CB2 1EZ, UK; fax: (+44) 1223 336 033; or e-mail: deposit@ccdc.cam.ac.uk.

Supplementary data associated with this article can be found, in the online version, at http://dx.doi.org/10.1016/j.poly.2012.04.004.

References

[1] For an outline see: Y.I. Baukov, S.N. Tandura, Hypervalent Compounds of Organic Germanium, Tin and Lead Derivatives, in: Z. Rappoport (Ed.), The Chemistry of Organic Germanium, Tin and Lead Compounds, vol. 2, John Wiley & Sons, West Sussex, 2002, p. 963.
[2] R. Cea-Olivares, V. García-Montalvo, M.M. Moya-Cabrera, Coord. Chem. Rev. 249 (2005) 859. and references therein cited.
[3] R.A. Varga, K. Jurkschat, C. Silvestru, Eur. J. Inorg. Chem. (2008) 708.
[4] D. Ocampo-Gutiérrez de Velasco, R. Sánchez Jiménez, S. Hernández-Orrtega, R. Alfredo Toscano, V. García-Montalvo, Polyhedron 29 (2010) 2435.
[5] D.G. Vargas-Pineda, T. Guardado, F. Cervantes-Lee, A.J. Meta-Magana, K.H. Pannell, Inorg. Chem. 49 (2010) 960.
[6] L. Pellerito, L. Nagy, Coord. Chem. Rev. 224 (2002) 111.
[7] S. González-Montiel, N. Andrade-López, V. García-Montalvo, J.A. Cogordan, J.G. Alvarado-Rodríguez, Eur. J. Inorg. Chem. (2006) 4752.
[8] J.G. Alvarado-Rodríguez, S. González-Montiel, N. Andrade-López, J.A. Cogordan, L.L. Lima-Ortiz, Polyhedron 29 (2010) 2283.
[9] D. Martínez-Otero, J.G. Alvarado-Rodríguez, J. Cruz-Borbolla, N. Andrade-López, T. Pandiyan, R. Moreno-Esparza, M. Flores-Alamo, J. Cantillo-Castillo, Polyhedron 33 (2012) 367. and references therein cited.
[10] S. González-Montiel, B. Flores-Chávez, J.G. Alvarado-Rodríguez, N. Andrade-López, J.A. Cogordan, Polyhedron 28 (2009) 467.
[11] S. González-Montiel, N. Andrade-López, J.G. Alvarado-Rodríguez, Eur. J. Inorg. Chem. (2006) 3762.
[12] J.G. Alvarado-Rodríguez, S. González-Montiel, N. Andrade-López, L.B. López-Feliciano, Polyhedron 26 (2007) 2929.
[13] B. Flores-Chávez, J.G. Alvarado-Rodríguez, N. Andrade-López, V. García-Montalvo, E. Aquino-Torres, Polyhedron 28 (2009) 782.
[14] Oxford Diffraction, CrysAlis software system, version 1.171.33.31. Oxford Diffraction Ltd., Abingdon, UK, 2009.
[15] SADABS: Area-Detector Absorption Correction, Siemens Industrial Automation, Inc., Madison, WI, 1996.
[16] SHEXTL 5.10 Bruker AXS, Inc., Madison. WI, USA, 1998.
[17] SPARTAŃ 08, Wavefunction, Inc., Japan Branch Officer, 2006–2008.
[18] F. Weigend, R. Ahlrichs, Phys. Chem. Chem. Phys. 7 (2005) 3297.
[19] B. Metz, H. Stoll, M. Dolg, J. Chem. Phys. 113 (2000) 2563.
[20] E. Cańces, B. Mennucci, J. Tomasi, J. Chem. Phys. 107 (1997) 3032.
[21] B. Mennucci, E. Cańces, J. Tomasi, J. Phys. Chem. B 101 (1997) 10506.
[22] Gaussian 09, Revision A.I., M.J. Frisch, G.W. Trucks, H.B. Schlegel, G.E. Scuseria, M.A. Robb, J.R. Cheeseman, G. Scalmani, V. Barone, B. Mennucci, G.A. Petersson, H. Nakatsuji, M. Caricato, X. Li, H.P. Hratchian, A.F. Izmaylov, J. Bloino, G. Zheng, J.L. Sonnenberg, M. Hada, M. Ehara, K. Toyota, R. Fukuda, J. Hasegawa, M. Ishida, T. Nakajima, Y. Honda, O. Kitao, H. Nakai, T. Vreven, J.A. Montgomery, Jr., J.E. Peralta, F. Ogliaro, M. Bearpark, J.J. Heyd, E. Brothers, K.N. Kudin, V.N. Staroverov, R. Kobayashi, J. Normand, K. Raghavachari, A. Rendell, J.C. Burant, S.S. Iyengar, J. Tomasi, M. Cossi, N. Rega, J.M. Millam, M. Klene, J.E. Knox, J.B. Cross, V. Bakken, C. Adamo, J. Jaramillo, R. Gomperts, R.E. Stratmann, O. Yazyev, A.J. Austin, R. Cammi, C. Pomelli, J.W. Ochterski, R.L. Martin, K. Morokuma, V.G. Zakrzewski, G.A. Voth, P. Salvador, J.J. Dannenberg, S. Dapprich, A.D. Daniels, Ö. Farkas, J.B. Foresman, J.V. Ortiz, J. Cioslowski, D.J. Fox, Gaussian, Inc., Wallingford CT, 2009.
[23] R.F. Bader, Atoms in Molecules: A Quantum Theory, Oxford University Press, Oxford, UK, 1994.
[24] AIM2000, version 1.0, Biegler-Köning, University of Applied Sciences, Bielefeld, Germany, 2000.
[25] J.C. Meurice, J.-G. Duboudin, M. Ratier, M. Pétraud, R. Willem, M. Biesemans, Organometallics 18 (1999) 1699.
[26] J. Otera, J. Organomet. Chem. 221 (1981) 57.
[27] J. Holecek, M. Nadvornik, K. Handlir, J. Organomet. Chem. 241 (1983) 177.
[28] B. Wrackmeyer, Modern Magnetic Resonance, Part 1, in: A. Graham Webb (Ed.), Springer, Netherlands, 2008, p. 461.
[29] N.W. Alcock, Bonding and Structure: Structural Principles in Inorganic and Organic Chemistry, Ellis Horwood, West Sussex, 1990.
[30] W.W. Porterfield, Inorganic Chemistry: A Unified Approach, 2nd ed., Academic Press, San Diego, Cal, 1993. p. 214.
[31] M. Draeger, J. Organomet. Chem. 251 (1983) 209.
[32] L. Pauling, The Nature of the Chemical Bond, 3rd ed., Cornell University Press, Ithaca, NY, 1960. p. 239.
[33] U. Kolb, M. Beuter, M. Gerner, M. Draeger, Organometallics 13 (1994) 4413.